AXAF Science Center

Harvard–Smithsonian
Center for Astrophysics

MEMORANDUM

April 15, 1998

To: ASC Calibration, AXAF CAT & HRC IPI

From: Daniel Patnaude, Deron Pease & Hank Donnelly

Subject: Spectral Fitting of HXDS Beam Normalization Detectors: Results for HRC Tests (Phase G)

1   Introduction

This memo describes the analysis of the HXDS Beam Normalization Detector (BND) data taken at XRCF during the testing of the HRC (Phase G). The HXDS consisted of five nearly identical Flow Proportional Counters (FPC) and one germanium Solid State Detector (SSD). Four of the FPCs were positioned around the High Resolution Mirror Assembly (HRMA), denoted as BND-HT, BND-HB, BND-HN, and BND-HS, for the top, bottom, north and south detectors respectively. The remaining FPC and SSD were positioned between the HRMA and the source, approximately 500 feet from the source. In general these two BNDs, denoted FPC-500 and SSD-500, were used only for beam-mapping. A typical measurement consisted of simultaneously exposing the four BNDs and the focal plane instrument. A large fraction of the measurements done for the High Resolution Camera (HRC) used either the Dual-Crystal Monochromator (DCM), or the High Resolution Erect Field Spectrometer (HIREFS) X-ray sources. The Electron Impact Point Source (EIPS) also was used, but its use was limited to low energy anodes such as Boron, Beryllium, and Carbon. Although this memo is limited to the analysis of the Phase G data the methods and software outlined herein are also applicable to the other testing Phases.

2   Method

The BND data arrived in the form of pulse-height histograms (*i.e.* total events versus pulse–height channel), also known as iterations. Each iteration was approximately 20 seconds long, thus producing several iterations per measurement. A summary file was also produced for each iteration, giving the dead time corrected count rate in a region of interest– a set of pulse height channels containing the energies of interest– defined by the HXDS operator. Using the measurement start and stop times, we summed the individual iterations to obtain

an aggregate histogram. This aggregate histogram was then converted into FITS format for use in the JMKmod (Jahoda-McCammon-Kramer model) developed by the Mission Support Team for use with the XSPEC software package.

2.1 The Input Model: JMKmod

The overall object of fitting the aggregate histograms was to extract an incident source spectrum in units of photons s^{-1} cm^{-2} keV^{-1}. The spectrum is composed of a series of spectral lines, represented as δ-functions, and a Kramer continuum component of the form,

$$N_c(E_\gamma)dE_\gamma = kZ\frac{(E_{max} - E_\gamma)}{E_\gamma}dE_\gamma \tag{1}$$

where E_{max} is the continuum cutoff energy, E_γ is the energy of the photon, and k is a constant.

The JMKmod contains several parameters for the detector (gain, Fano factor, Polya parameter, *etc*), and several independent parameters for the XSS (line energy, filter models and thicknesses *etc.*). The model incident spectrum detailed above is convolved with a parametrized version of the detector response and the resultant simulated output spectrum is compared directly to the BND data (Edgar 1997).

Although the JMKmod does not contain any background components, XSPEC allows us to linearly combine models. We independently fit the detector background at each energy, using a power-law for low (1-40) channel noise and a broad Gaussian for the remainder, and applied these corrections to the model.

For the monochromators, the continuum contribution to the integrated flux is less than the background rate. For HRC measurements, the problem then reduces to finding the flux in a set of spectral lines.

2.2 Fitting the PHA's

The general procedure for fitting BND spectra data taken during the HRC testing (Phase–G) is to create a "template" for each detector/energy configuration, detailing the various detector parameters common to all tests at that particular energy.

For each energy, the Polya parameter, Fano factor, principal line normalization and background parameters are assumed constant. The background parameters probably vary weakly as a function of gain and temperature, but are held fixed for ease of calculation.

Most of the spectra have a feature called a "shelf" which lies between channel 0 and the peak of the distribution and is approximately flat. This "shelf" is due to incomplete charge collection (see Edgar *et al.* 1997 for a more complete definition), and its normalization along with the detector gain and the model's global normalization are allowed to vary.

A common problem with all of our BND spectra is the low signal-to-noise due to intrinsically weak sources being run at low currents. Cash (1979) has shown that a χ^2 minimization criterion is inappropriate if the observed data has any bins with few counts, due to the underestimation of the weights of the differences between the data and the fit in the wings (Bevington 1992). A better method involves using a maximum likelihood criterion or C-statistic. We found that the χ^2 fits underestimated the normalization parameters by as much as $\sim 20\%$. In conjunction with the MST, we have implemented the C-statistic in XSPEC v10. This is available from the ASC Calibration web site (asc.harvard.edu/cal.html).

The data are then batch-fit using a common template. Two files are output for each individual fit: the first file contains all the model information, as well as the PHA filename, response matrix, and the channels used; the second logs the fit, including the fit quality, and contains the information necessary to derive the detected count rates and incident fluxes. An example log file can be found in Appendix A.

The results are combined into an extensive RDB table containing all the fit information for each runid. This includes the fractional normalizations for all lines fit, as well as the global normalization. The fractional shelf normalization is not included, as this is folded into the calculation of the global normalization. The table also contains ancillary information such as the model name, log file name, and specific information such as the detector gain and the date that the fit was performed. This file is the root level product used for the generation of incident fluxes in the analysis of focal plane data.

2.3 Calculating the Incident Flux

The flux incident on the HRMA opening as measured by a given BND for the ith line in units of *photons* cm^{-2} s^{-1} is calculated using the following prescription:

$$F_{i,BND-HT...} = \frac{R_{i,BND-HT...}}{\eta_{i,BND-HT...} \times A_{BND-HT...}} \tag{2}$$

where $R_{i,BND-HT...}$ and $\eta_{i,BND-HT...}$ are the derived count rate and quantum efficiency respectively for the line and detector of interest and $A_{BND-HT...}$ is the open area of the appropriate detector. The derived count rate is the product of the model's global normalization (in units of counts per second) and the fractional normalization (which is dimensionless) of the ith line:

$$R_{i,BND-HT...} = N_{global,BND-HT...} \times N_{i,BND-HT...}. \tag{3}$$

The uncertainty in the derived rates, $\sigma_{R_{i,BND-HT...}}$, is found via a standard quadrature sum of the errors in the normalizations:

$$\sigma_{R_{i,BND-HT...}} = \left\{ R_{i,BND-HT...}^2 \times \left[\left(\frac{\sigma_{N_{global,BND-HT...}}}{N_{global,BND-HT...}} \right)^2 + \left(\frac{\sigma_{N_{i,BND-HT...}}}{N_{i,BND-HT...}} \right)^2 \right] \right\}^{\frac{1}{2}}. \qquad (4)$$

This is then combined with an estimated 5% uncertainty in $\eta_{i,BND-HT...}$ (Edgar 1997), to give the final uncertainty in the incident fluxes. The uncertainty in the FPC aperture area is known, but does not contribute significantly to the overall error. The quantum efficiencies of the four BND-Hs are plotted in Figure 1.

2.4   Correcting for Beam Non-Uniformities

The analysis of many of the tests was complicated by spatial and spectral non-uniformities. Prior to some of the tests, a set of Beam Uniformity (BU) maps were taken by the AXAF Project Science group. A set of polynomials and Gaussians were fit to these maps, resulting in a modeled flux at each position and energy. Unfortunately the mapping procedure was not performed at all energies used for the HRC.

For the cases where a BU map was performed either at the energy of interest or near to it, for each line detected Project Science modeled the flux incident on each shell-quadrant combination per unit source current– $\tilde{F}_i(q, s, I)$ in units of *photons cm^{-2} s^{-1} mA^{-1}*. Asscociated with these fluxes were the incident fluxes per unit source current predicted in each of the BND-H's ($\tilde{F}_{i,BND-HT}, \tilde{F}_{i,BND-HB}$...). Summing over these fluxes multiplied by the appropriate HRMA area produces a modeled *output* count rate per unit source current ($\mathcal{F}_i(I)$ *photons s^{-1} mA^{-1}*).

$$\mathcal{F}_i(I) = \sum (A_i(q, s) \times \tilde{F}_i(q, s, I)) \qquad (5)$$

the errors are independent and added in quadrature.

By comparing the measured input flux for a given BND fitted above in Section 2.3 to the normalized flux, we derived a measure of the source current in milliAmps,

$$\lambda_{i,BND-HT...} = \frac{F_{i,BND-HT...}}{\tilde{F}_{i,BND-HT...}} \qquad (6)$$

which we then applied to the output modeled count rate per unit source current,

$$\mathcal{F}_{i,BND-HT...} = \mathcal{F}_i(I) \times \lambda_{i,BND-HT...} \qquad (7)$$

giving an output count rate in *photons s^{-1}*. Again the uncertainty in the measured flux was added in quadrature to the overall error.

This produced four measurements of the output count rate which were then combined via a weighted average. We note that we found a systematic bias in the scaling factor of the north detector which was an artifact of the polynomial fits (Swartz 1998),

$$\mathcal{F}_i = \frac{\sum \mathcal{F}_{i,BND-H*}/\sigma_{i,BND-H*}^2}{\sum (1/\sigma_{i,BND-H*}^2)} \qquad (8)$$

and the total weighted error was:

$$\sigma_i^2 = \frac{1}{\sum 1/\sigma_{i,BND-H*}^2} \tag{9}$$

For measurements where there was no nearby BU data or it was on the other side of an edge, we employed a much more primitive method and used the average flux from the four BND's

$$\overline{F}_i = \frac{\sum F_{i,BND-H*}}{N_{det}} \tag{10}$$

times the total HRMA effective area to produce the output count rate

$$\mathcal{F}_i = \overline{F}_i \times A_i \tag{11}$$

with an RMS error of:

$$\sigma_i^2 = \sum \frac{\sigma_{i,BND-H*}^2}{N_{det}^2}. \tag{12}$$

3 Results

3.1 HIREFS

The measurements conducted with the HIREFS suffered from two major problems. First, was that the beam intensity was strongly dependent upon position. Table 1 lists the derived flux for each of the BND-H's from the fits shown in Figure 2. The fluxes strong dependence upon azimuth is immediately obvious. An independent analysis of the beam mapping measurements done by Swartz (1997) suggests a further radial dependence not detectable in these results.

The second problem with the HIREFS data was the common occurrence of contaminating lines, i.e. those other than at the energy of interest. Figure 3 shows a test conducted at an energy of 0.905 keV. In this case, there is a line at 1.810 keV due to a 2nd order line and/or a Tungsten M line. Table 2 gives the derived flux at each energy for each detector. This data is representative of the spectral as well as spatial variations which were common in the HIREFS data.

Between 1.770 and 1.830 keV, there was a group of Tungsten lines (W-$M_{\alpha_1,\alpha_2,\beta}$) which scattered off the HIREFS reflection gratings, appearing along with the desired line. For tests conducted within this energy range, the spectra were substantially broadened, although dominated by the line of interest . This complicated any effort to independently fit the various lines. Fortunately, the HRMA effective area, FPC quantum efficiency, and the quantum efficiency of the HRC nominally vary slowly across this range. This allowed us to model the convolved lines as a single composite line without misrepresenting the flux, other than by increasing the uncertainty in the energy. However, for the analysis of the HRC data this has a minimal impact due to the limited energy resolution of the HRC.

3.2   DCM

Due to the reduced quantum efficiency of the HRC in the range from 3-10 keV, the DCM was run at a much higher flux than the HIREFS. This led to generally higher counting statistics for this data. The DCM also suffered much less than the HIREFS from spatial non-uniformities in the beam. Although the DCM was optimized to minimize the flux in the 2nd order, there were minor contributions from 3rd and higher orders. Figure 4 is representative of the incident spectrum at a DCM energy of 2.560 keV. Table 3 gives the derived flux from each BND.

At energies above the Ar-K edge at 3.205 keV, escape peaks begin to form in the spectrum. These occur when fluorescent photons escape completely from the gas before reaching the active region. This limits the number of secondary electron-ion pairs produced (Jahoda & McCammon 1988). Because these are real events, they must be included in the calculation of the detected count rate (and hence the detected flux). The JMKmod does not include an escape peak component, so this was modeled by fitting the escape peak as a separate line and then appropriately recombining the results. Figure 5 is a DCM test done at 4.960 keV. Table 4 gives the derived flux for this test.

3.3   EIPS

The EIPS with Boron, Beryllium and Carbon anodes was used in a limited number of measurements. Although the point sources do not suffer from the same beam uniformity problems that the monochromators do, they do generate a contaminating continuous spectrum up to the high voltage cutoff along with the line of interest. Blocking filters were used to remove the continuum photons, which unfortunately also depleted the flux in the line. This led to a trade off between spectral purity and good counting statistics.

This was further complicated by the limited response of the FPC's ($\sim$ 15%) at these energies, as well as the location of the peak of the PHA in the extreme low end of the available channels which are typically dominated by amplifier noise. Overall, the low energy EIPS data was subject to the largest uncertainties in our fitting process.

4   Conclusion

The fits detailed here have been used to study the combined effective area of the HRMA and HRC as well as the Count Rate Linearity behavior of the HRC. These results are detailed elsewhere (Patnaude *et al.* 1998, Pease & Donnelly 1998).

Our work has led to results in excellent agreement with previous work (Kraft *et al.* 1997; Kenter *et al.* 1997; Edgar *et al.* 1997), leading us to be confident that we have found the best possible set of fit parameters for each measurement while reducing the uncertainties in the final results.

Future efforts will go towards exploring the "physicality" of the fit parameters (e.g. Fano

and Polya factors), by comparing the results across all of the fits for a given energy. The fits are relatively insensitive to variations in these parameters, producing the same line and global normalizations to within 1%. More importantly we plan to continue refining/reducing the error bars via the inclusion of more complete BU data.

5   References

Cash, W. 1979, ApJ, 228, 939.

Bevington, P.R., & Robinson, D.K. 1992, *Data Reduction and Error Analysis for the Physical Sciences* (New York: McGraw Hill).

Edgar, R., Tsiang, E.Y., Tennant, A., Vitek, S. & Swartz, D. 1997 "Spectral Fitting in AXAF Calibration Detectors," in *Grazing Incidence and Multilayer X–Ray Optical Systems*, eds. R.B. Hoover and A.B. Walker, *Proc. SPIE* **3113**, 124.

Edgar, R. 1997, *private communication*.

Jahoda, K. & McCammon, D, 1988, Nuclear Instr. and Methods, A272, 800.

Kenter, A.T, Chappel, J.H., Kraft, R.P., Meehan, G.R., Murray, S.S., Zombeck, M.V., Fraser, G. , Pearson, J.F., Lees, J.E., Brunton, A.N., Pearce, S.E., Barbera, M., Collura, A. & Serio, S. 1997, "Performance and Calibration of the AXAF High Resolution Camera I: Imaging Readout", *Proc. SPIE*, **3114**

Kraft, R.P., Chappel, J.H., Kobayashi, K., Kenter, A.T., Meehan, G.R., Murray, S.S., Zombeck, M.V., Fraser, G.W., Pearson, J.F., Lees, J.E., Brunton, A.N., Pearce, S.E., Barbera, M., Collura, A. & Serio, S. 1997, "Performance and Calibration of the AXAF High Resolution Camera II: Spectroscopic Detector", *Proc. SPIE*, **3114**,

Patnaude, D., Pease, D., Donnelly, R.H., Juda, M., Jones, C., Murray, S.S., Zombeck, M.V., Kraft, R., Kenter, A., Meehan, G., Elsner, R. & Swartz, D. 1998, *in preparation*.

Pease, D., Donnelly, H. 1998, ASC Memorandum, "Count Rate Linearity of the AXAF High Resolution Camera (HRC)".

Swartz, D. 1997, *private communication*.

Swartz, D. 1998, *private communication*.
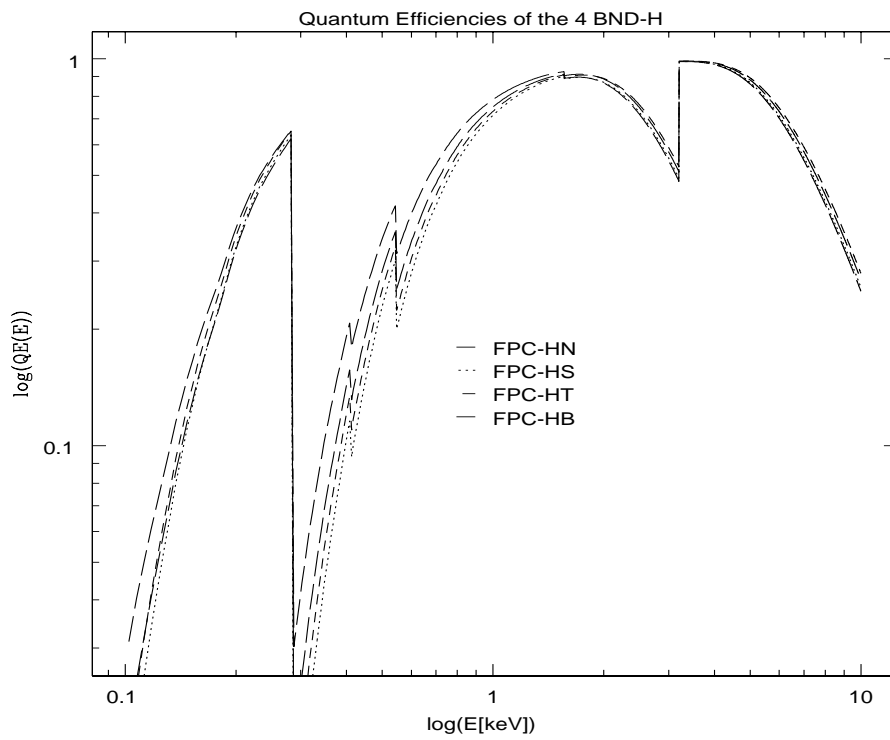
Figure 1: Preliminary Quantum Efficiencies for the 4 BNDs at the HRMA entrance. These curves were generated from the calibration of the ACIS–I3 Chip.
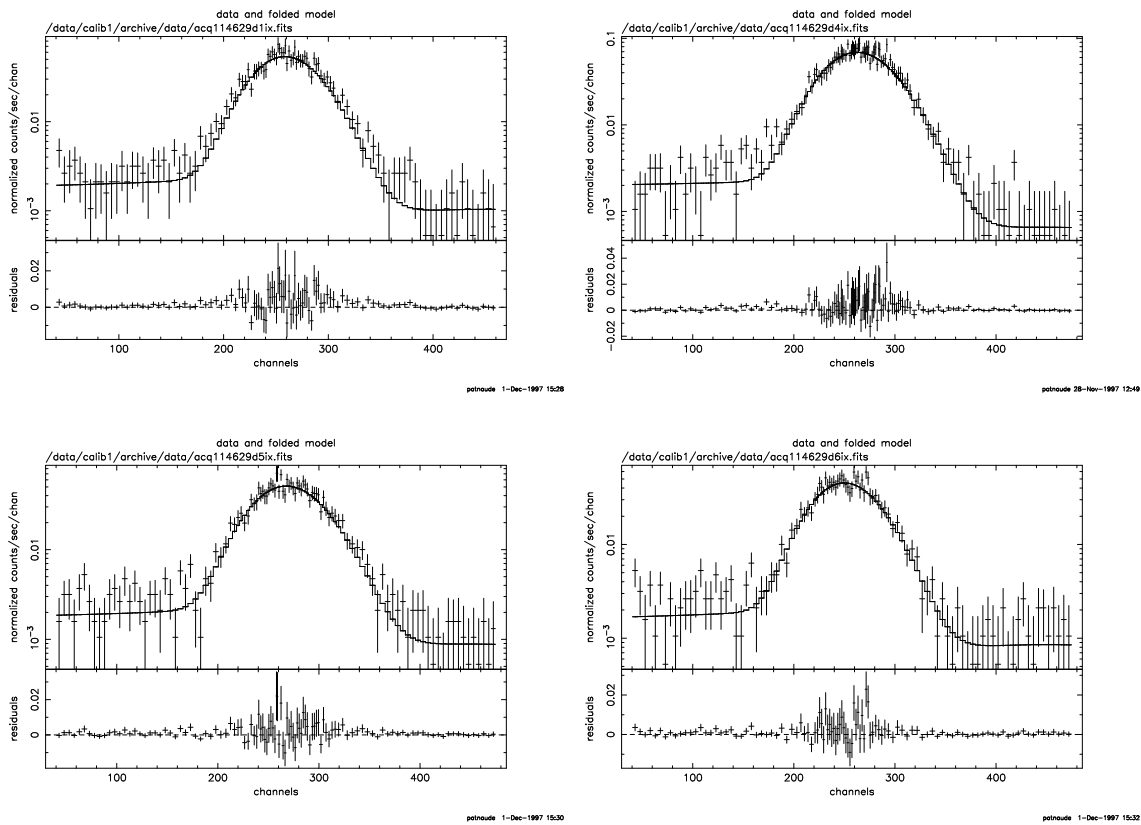
Figure 2: HIREF spectrum at 1.810 keV for the 4 BNDs. In clockwise order the designations are FPC-HN, FPC-HS, FPC-HB, and FPC-HT. The scales are representative of the spatial intensity variations.

Table 1: Derived Flux at 1.810 keV
Test: G-IHI-EA-1.067

Detector	$F_{1.810}$ (photons cm^{-2} s^{-1})
BND-HN	0.160 ± 0.009
BND-HS	0.214 ± 0.012
BND-HT	0.165 ± 0.009
BND-HB	0.140 ± 0.008
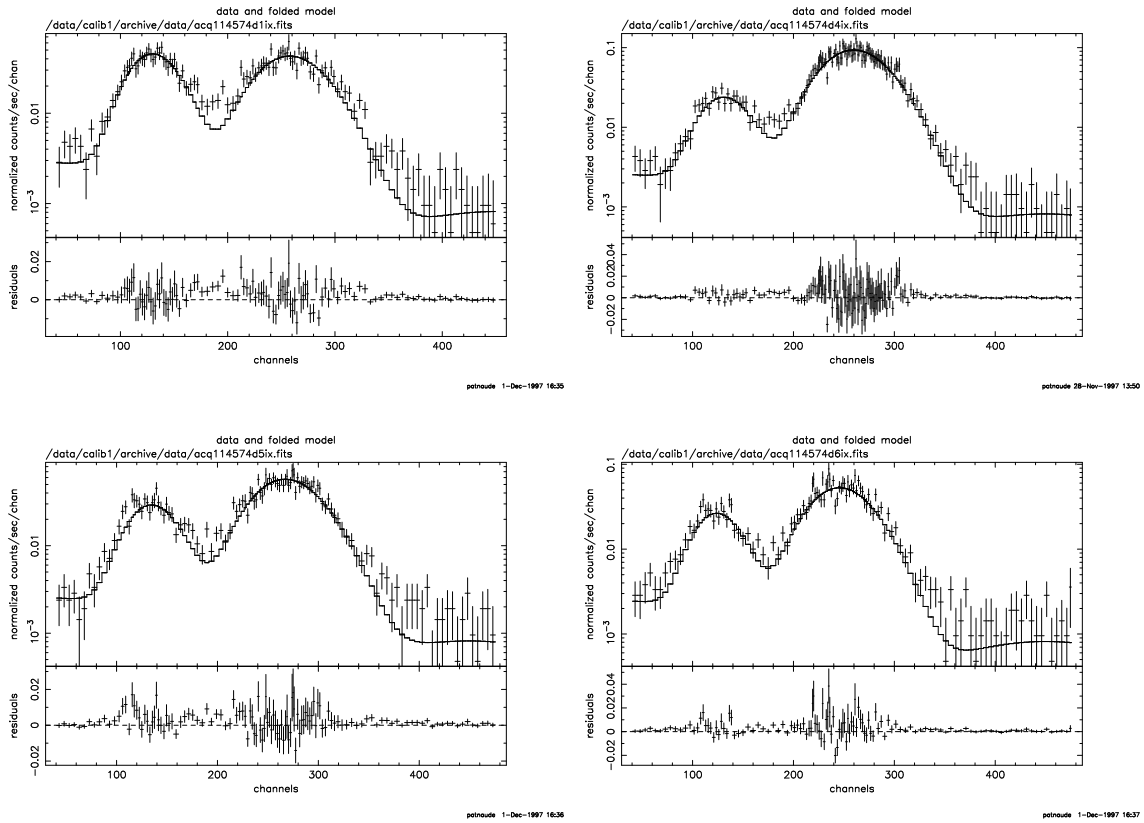
Figure 3: HIREFS spectrum at 0.905 keV for the 4 BNDs. There is significant contamination at ~ 1.810 keV, due to a 2nd order line and/or a Tungsten M line. In clockwise order the designations are FPC-HN, FPC-HS, FPC-HB, and FPC-HT. There is clearly an azimuthal dependence in the relative intensities between the two lines.

Table 2: Derived Flux at 0.905 keV
Test: G-IHI-EA-1.033

Detector	$F_{0.905}$ (photons cm^{-2} s^{-1})	$F_{1.810}$ (photons cm^{-2} s^{-1})
BND-HN	0.113 ± 0.007	0.124 ± 0.009
BND-HS	0.063 ± 0.005	0.273 ± 0.025
BND-HT	0.081 ± 0.005	0.173 ± 0.014
BND-HB	0.065 ± 0.004	0.149 ± 0.013
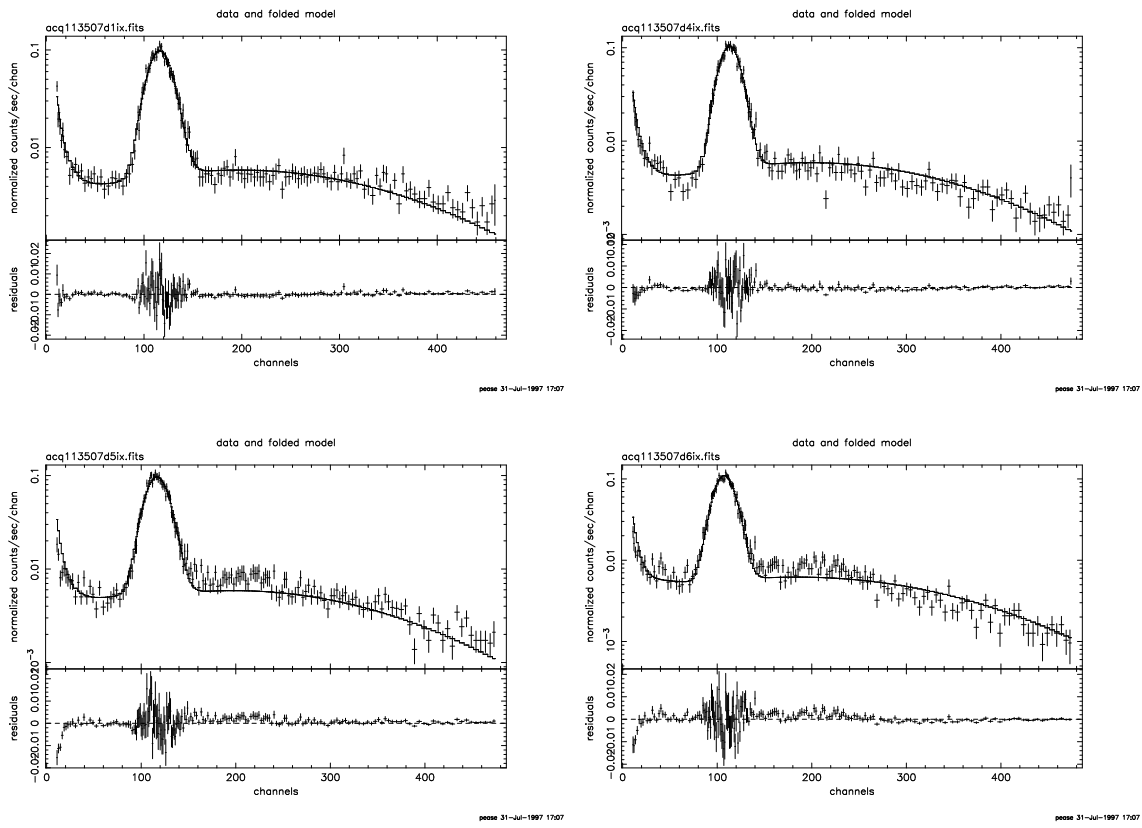
Figure 4: DCM spectrum at 2.560 keV for the 4 BNDs. In clockwise order the designations are FPC-HN, FPC-HS, FPC-HB, and FPC-HT.

Table 3: Derived Flux at 2.560 keV
Test: G-IHI-EA-1.119

Detector	$F_{2.560}$ (photons cm^{-2} s^{-1})
BND-HN	0.115 ± 0.006
BND-HS	0.116 ± 0.006
BND-HT	0.118 ± 0.006
BND-HB	0.125 ± 0.007
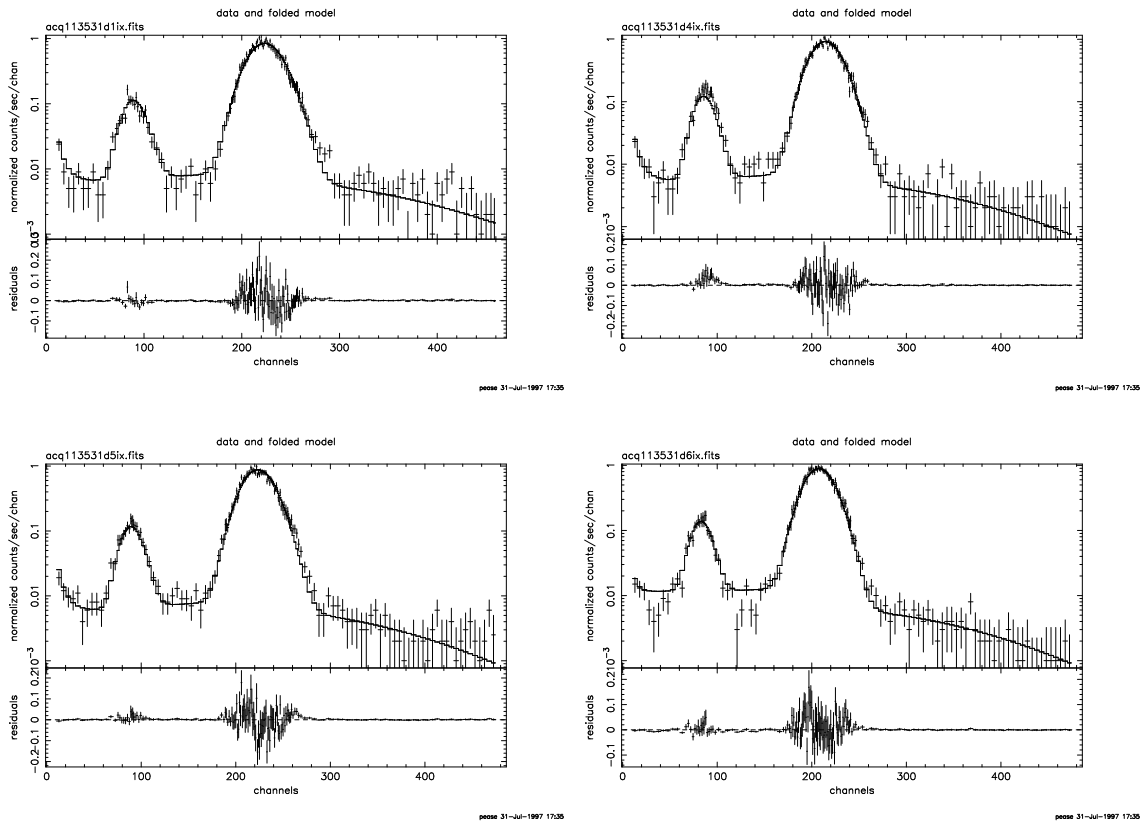
Figure 5: DCM spectrum at 4.960 keV for the 4 BNDs. There is an escape peak at $\sim$ 2 keV which is modeled as a separate line in XSPEC. In clockwise order the designations are FPC-HN, FPC-HS, FPC-HB, and FPC-HT.

Table 4: Derived Flux at 4.960 keV
Test: G-IHI-EA-1.085

Detector	$F_{4.960}$ (photons cm^{-2} s^{-1})
BND-HN	1.379 ± 0.072
BND-HS	1.395 ± 0.073
BND-HT	1.346 ± 0.071
BND-HB	1.371 ± 0.072

A   Sample Log File

Below is a sample log file generated by XSPEC using JMKmod. This fit employs an 8 line
model with a principal energy, E_0, of 0.392 keV. There is considerable contamination from
2nd, 3rd, and 4th orders. There is also possibly some contamination from a 5th order, but
because this is just above the Tungsten M_β line at 1.835 keV, the spectrum is dominated by
scattering from the Tungsten line.

```
!xspec 18:57:43 12-Nov-97
XSPEC> show all
 18:57:46 12-Nov-97
 Fit statistic in use is Chi-Squared
 Minimization technique is Lev-Marq
 Weighting method is standard
  Convergence criterion =      1.0000000000000D-02
 Querying enabled
 Prefit-renorming enabled
 Solar abundance table is angr
 Log file : acq114537d4ix.log

 Information for file    1
  belonging to plot group   1, data group   1
 telescope = HXDS , instrument = fpc_hs  channel type = PHA
  Current data file: acq114537d4ix.fits
  No current background
  No current correction
  Response (RMF) file    : /home/edgar/diag512.rmf
  Auxiliary (ARF) file   : none
  Noticed channels    36 to   474
  Spectral bins        1 to   439
  File integration time      3792.
     and effective area      1.000
  File observed count rate     3.434    +/-3.00988E-02 cts/s
  Model predicted rate :    3.327


    --------------------------------------------------------------------------------
    --------------------------------------------------------------------------------
  mo = jmkmod8[1] + powerlaw[2] + gaussian[3]
  Model Fit Model    Component      Parameter    Value
  par   par comp
    1    1    1          jmkmod8      fano        0.129855     frozen
    2    2    1          jmkmod8      polyah      1.21300      frozen
    3    3    1          jmkmod8      E_offset          0.     frozen
    4    4    1          jmkmod8      i_pot       2.800000E-02 frozen
```

```
 5    5   1        jmkmod8     gain       3.90000        frozen
 6    6   1        jmkmod8     ch_off          0.        frozen
 7    7   1        jmkmod8     broad           0.        frozen
 8    8   1        jmkmod8     d_gain          0.        frozen
 9    9   1        jmkmod8     nchan      512.000        frozen
10   10   1        jmkmod8     sestype    1.00000        frozen
11   11   1        jmkmod8     contin          0.        frozen
12   12   1        jmkmod8     econt      10.0000        frozen
13   13   1        jmkmod8     contnorm   1.00000        frozen
14   14   1        jmkmod8     E_max      10.0000        frozen
15   15   1        jmkmod8     E_min      1.000000E-02 frozen
16   16   1        jmkmod8     E_char     2.00000        frozen
17   17   1        jmkmod8     E_width    0.100000       frozen
18   18   1        jmkmod8     nInt       512.000        frozen
19   19   1        jmkmod8     temper     15.0000        frozen
20   20   1        jmkmod8     pressure   400.000        frozen
21   21   1        jmkmod8     argrat     0.900000       frozen
22   22   1        jmkmod8     shelfsw         0.        frozen
23   23   1        jmkmod8     t1norm          0.        frozen
24   24   1        jmkmod8     t1par      0.999000       frozen
25   25   1        jmkmod8     t2norm          0.        frozen
26   26   1        jmkmod8     t2par      1.00100        frozen
27   27   1        jmkmod8     shelfnm    5.000000E-03 frozen
28   28   1        jmkmod8     pulser          0.        frozen
29   29   1        jmkmod8     pulsepos   100.000        frozen
30   30   1        jmkmod8     pulsesig   1.00000        frozen
31   31   1        jmkmod8     pulsenrm   1.00000        frozen
32   32   1        jmkmod8     numcomp    8.00000        frozen
33   33   1        jmkmod8     numfil     6.00000        frozen
34   34   1        jmkmod8     pileup          0.        frozen
35   35   1        jmkmod8     pilepar    1.00000        frozen
36   36   1        jmkmod8     bfield     14500.0        frozen
37   37   1        jmkmod8     current    1.00000        frozen
38   38   1        jmkmod8     incline         0.        frozen
39   39   1        jmkmod8     abswitch        0.        frozen
40   40   1        jmkmod8     phi        135.400        frozen
41   41   1        jmkmod8     theta      40.2000        frozen
42   42   1        jmkmod8     shell      12.0000        frozen
43   43   1        jmkmod8     E_line1    0.391970       frozen
44   44   1        jmkmod8     E_line2    0.783940       frozen
45   45   1        jmkmod8     E_line3    1.17591        frozen
46   46   1        jmkmod8     E_line4    1.56788        frozen
47   47   1        jmkmod8     E_line5    1.77800        frozen
48   48   1        jmkmod8     E_line6    1.83490        frozen
49   49   1        jmkmod8     E_line7    2.00000        frozen
```

50	50	1	jmkmod8	E_line8	2.10000	frozen
51	51	1	jmkmod8	E_norm1	1.00000	frozen
52	52	1	jmkmod8	E_norm2	3.86796	+/- 0.19462
53	53	1	jmkmod8	E_norm3	6.18836	+/- 0.28804
54	54	1	jmkmod8	E_norm4	1.64623	+/- 0.11905
55	55	1	jmkmod8	E_norm5	0.	frozen
56	56	1	jmkmod8	E_norm6	0.645696	+/- 0.68111E-01
57	57	1	jmkmod8	E_norm7	0.	frozen
58	58	1	jmkmod8	E_norm8	0.	frozen
59	59	1	jmkmod8	src1	35.0000	frozen
60	60	1	jmkmod8	src2	6.00000	frozen
61	61	1	jmkmod8	src3	2.00000	frozen
62	62	1	jmkmod8	src4	19.0000	frozen
63	63	1	jmkmod8	src5	38.0000	frozen
64	64	1	jmkmod8	src6	45.0000	frozen
65	65	1	jmkmod8	srcthk1	0.	frozen
66	66	1	jmkmod8	srcthk2	0.	frozen
67	67	1	jmkmod8	srcthk3	2.000000E-06	frozen
68	68	1	jmkmod8	srcthk4	1.065000E-04	frozen
69	69	1	jmkmod8	srcthk5	5.36000	frozen
70	70	1	jmkmod8	srcthk6	0.	frozen
71	71	1	jmkmod8	norm	0.230099	+/- 0.10028E-01
72	72	2	powerlaw	PhoIndex	2.75000	frozen
73	73	2	powerlaw	norm	100.000	frozen
74	74	3	gaussian	LineE	400.000	frozen
75	75	3	gaussian	Sigma	100.000	frozen
76	76	3	gaussian	norm	0.200000	frozen

```
       --------------------------------------------------------------------
       --------------------------------------------------------------------
 Chi-Squared =       514.0     using   439 PHA bins.
 Reduced chi-squared =       1.184
XSPEC> log none
```